Electronic Supplementary Material (ESI) for Journal of Materials Chemistry A.

MXene driven in-situ construction of hollow core-shelled $Co_3V_2O_8$@$Ti_3C_2T_x$ nanospheres for high performance all-solid-state asymmetric supercapacitors

Ji Zhou [a], Binbin Liu [a], Lina Zhang [b], Qian Li [a], Caixia Xu [a,*] and Hong Liu [a,c]

[a] *Institute for Advanced Interdisciplinary Research (iAIR), Collaborative Innovation Center of Technology and Equipment for Biological Diagnosis and Therapy in Universities of Shandong, School of Chemistry and Chemical Engineering, University of Jinan, Jinan 250022, Shandong Province, China*

[b] *Shandong Provincial Key Laboratory of Preparation and Measurement of Building Materials, University of Jinan, Jinan, Shandong 250022, China*

[c] *State Key Laboratory of Crystal Materials, Shandong University, Jinan 250100, Shandong Province, China*

[*]Corresponding author.

E-mail address: chm_xucx@ujn.edu.cn (C. Xu)

Electrochemical measurements

The electrochemical measurements for cyclic voltammetry (CV), galvanostatic charge-discharge (GCD), and electrochemistry impedance spectroscopy (EIS) were performed on an electrochemical workstation (CHI 760E). The performance of a single electrode was tested using a three-electrode system with the working electrode, Pt foil as the counter electrode, and Hg/HgO as the reference electrode. The CV and GCD were implemented in the potential window of 0–0.55 V, and EIS was recorded in the frequency range from 0.01 to 100 kHz. The solid-state asymmetric supercapacitor (ASC) device was assembled by using AC coated on the nickel foam as the negative electrode and polyvinyl alcohol (PVA)/KOH gel as the electrolyte and separator, in which the mass of the $Co_3V_2O_8$@$Ti_3C_2T_x$ and AC electrodes were fixed at 1:1 in accordance with the charge balance theory. The PVA/KOH polymer gel was obtained by adding 1.0 g PVA into 10 mL of deionized water under continuous stirring at 85 °C until the solution became transparent followed by dissolving 0.5 g KOH.

The specific capacitance, energy density, and power density were calculated by Equations S1, S2, and S3 listed as below:

$$C = \frac{I \times \Delta t}{\Delta V \times S} \quad \text{(Equation S1)}$$

$$E = \frac{I \times \Delta t \times V}{7.2 \times S} \quad \text{(Equation S2)}$$

$$P = \frac{3.6 \times E}{\Delta t} \quad \text{(Equation S3)}$$

where C (mF cm^{-2}) is the areal capacitance, I (mA) is the discharge current, Δt (s) is the discharge time, ΔV (V) is the potential window exclusive of the IR drop, S (cm^{-2}) is the active area of the electroactive materials, E (μWh cm^{-2}) is the energy density, and P (mW cm^{-2}) is the power density.

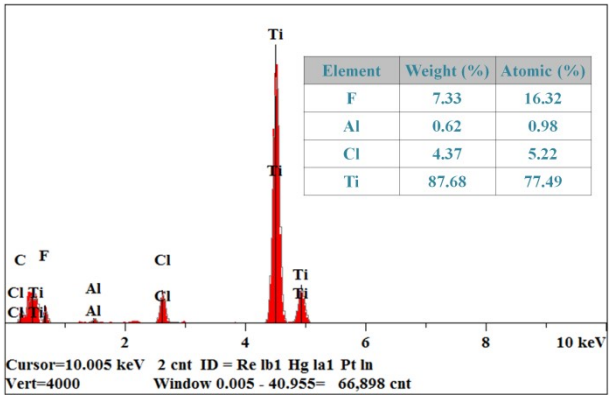

Element	Weight (%)	Atomic (%)
F	7.33	16.32
Al	0.62	0.98
Cl	4.37	5.22
Ti	87.68	77.49

Figure S1. EDS data of exfoliated $Ti_3C_2T_x$ MXene in HCl/LiF solution.

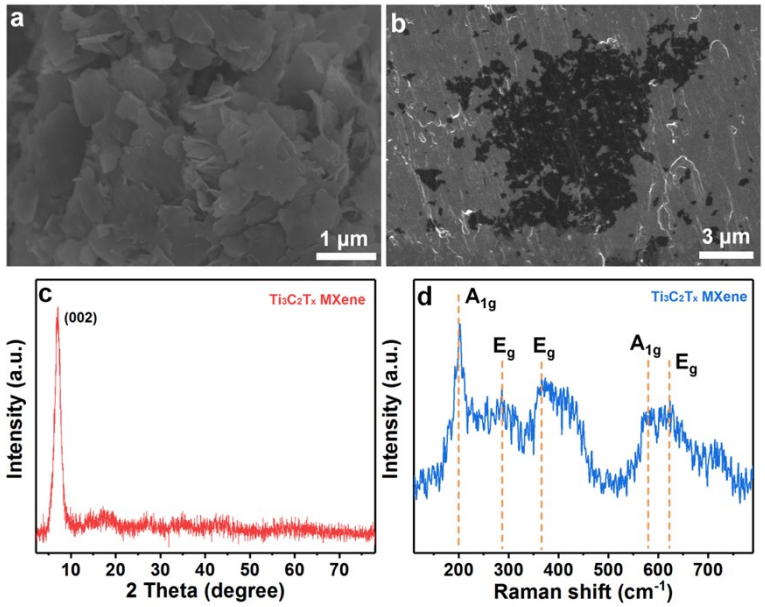

Figure S2. (a, b) SEM images, (c) XRD pattern, (d) Raman spectrum of exfoliated $Ti_3C_2T_x$ MXene.

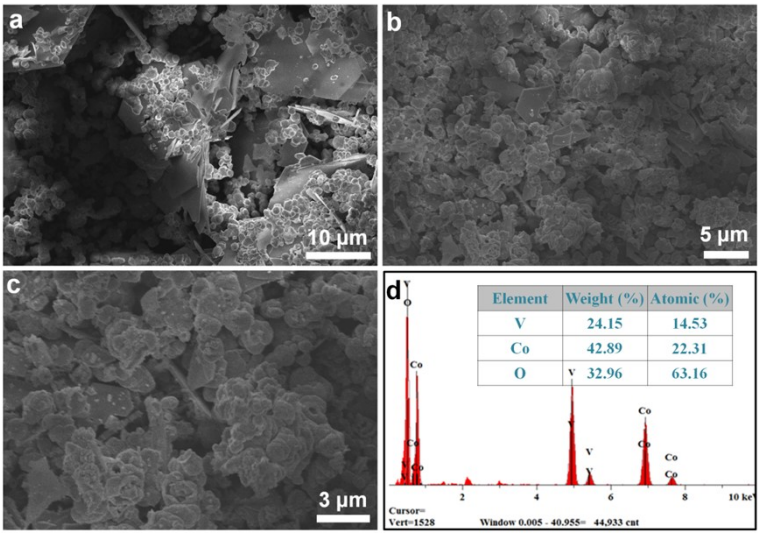

Figure S3. (a, b) SEM images, (c) EDS data of pure $Co_3V_2O_8$ sample.

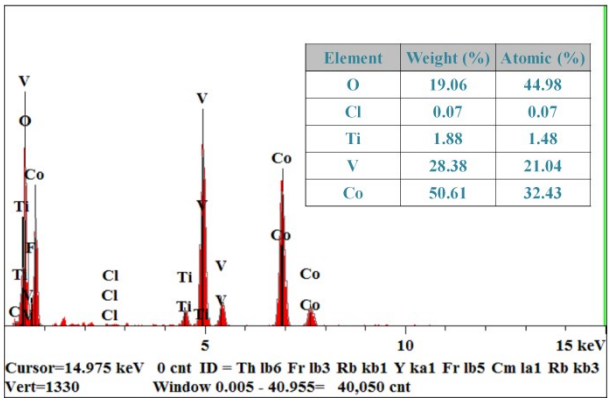

Figure S4. EDS data of $Co_3V_2O_8$@$Ti_3C_2T_x$-1.5 composite.

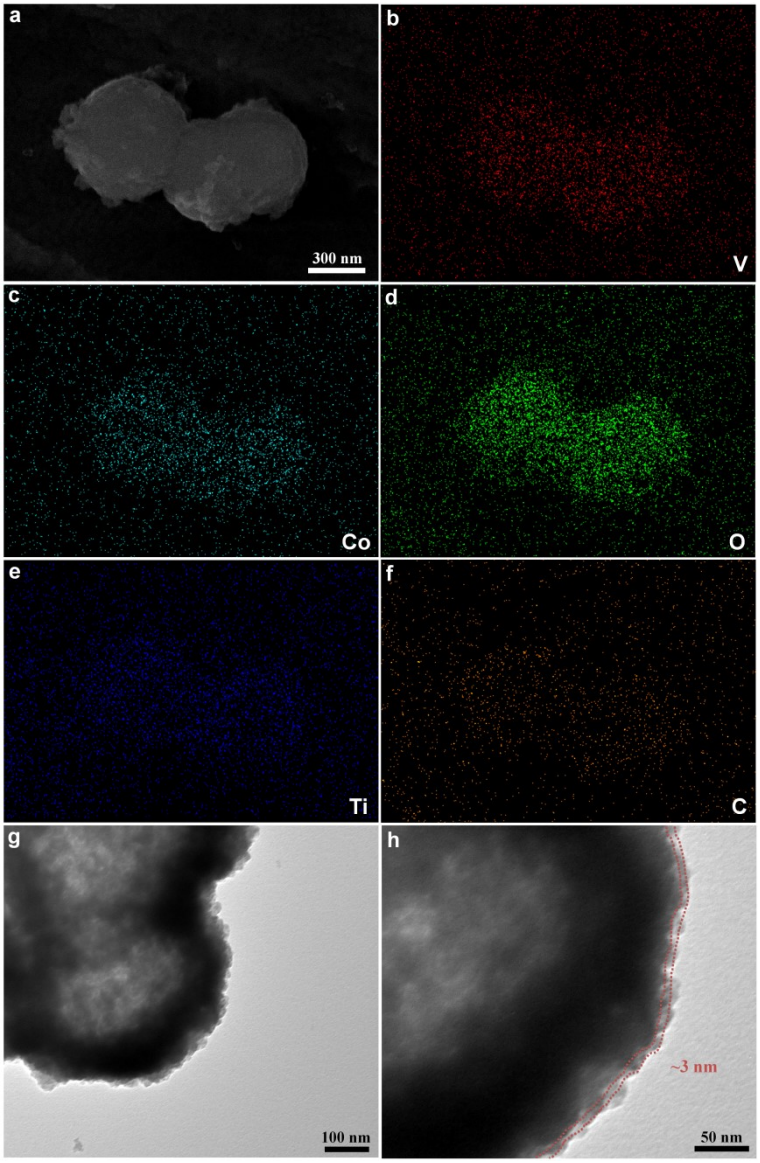

Figure S5. The SEM element mapping of selected area of (a) $Co_3V_2O_8$@$Ti_3C_2T_x$-1, (b) V, (c) Co, (d) O, (e) Ti, and (f) C element; (g, h) TEM images of $Co_3V_2O_8$@$Ti_3C_2T_x$-1 sample.

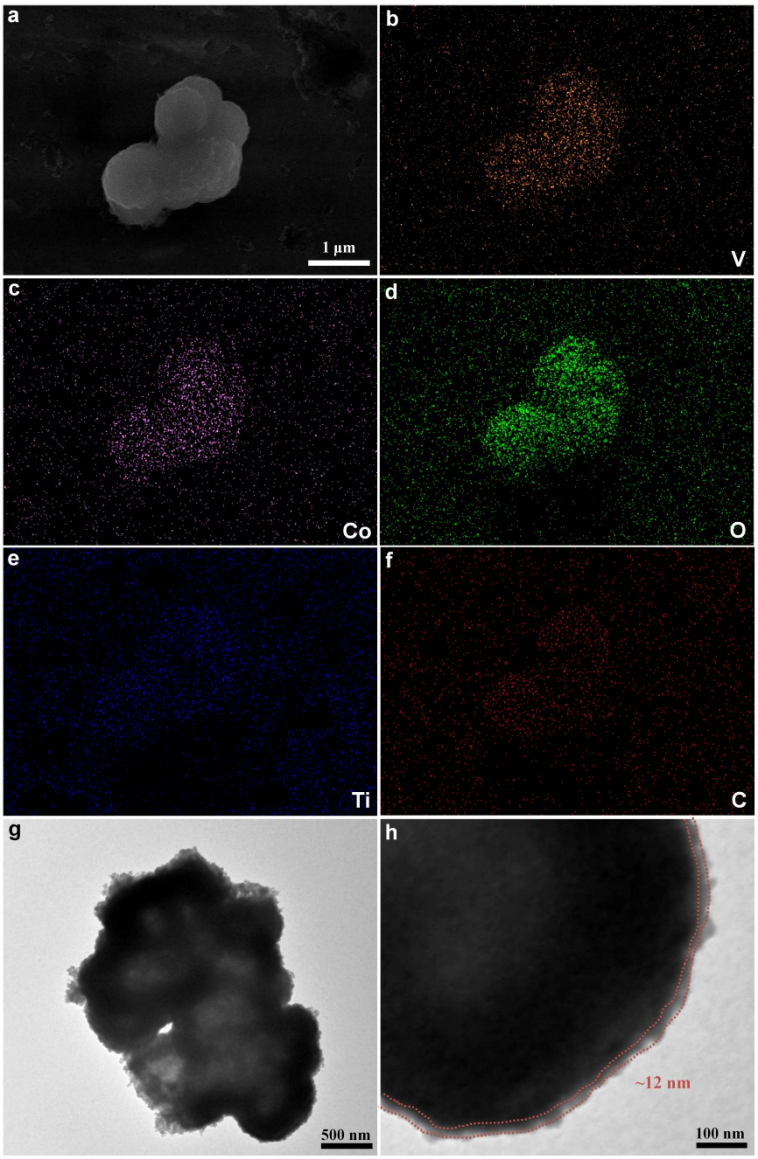

Figure S6. The SEM element mapping of selected area of (a) $Co_3V_2O_8$@$Ti_3C_2T_x$-2, (b) V, (c) Co, (d) O, (e) Ti, and (f) C element; (g, h) TEM images of $Co_3V_2O_8$@$Ti_3C_2T_x$-2 sample.

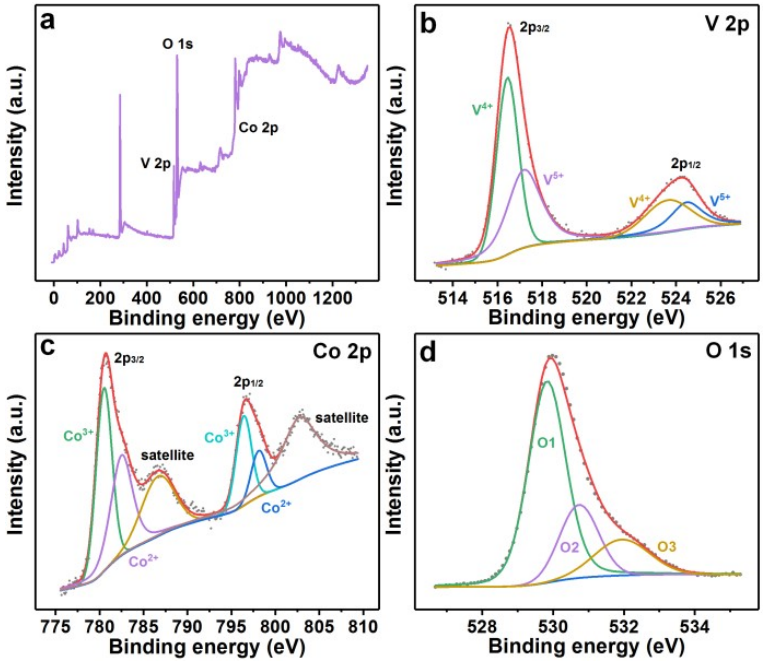

Figure S7. XPS data of pure $Co_3V_2O_8$ sample.

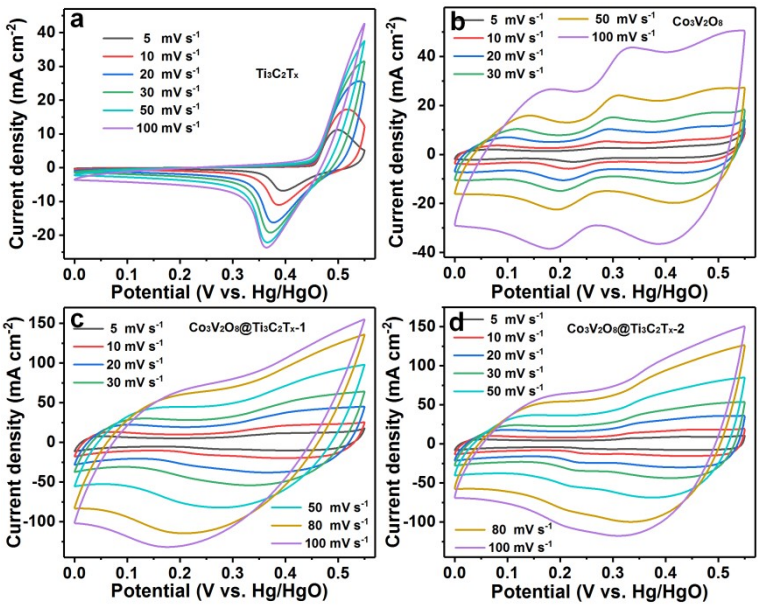

Figure S8. CV curves for (a) $Ti_3C_2T_x$, (b) pure $Co_3V_2O_8$, (c) $Co_3V_2O_8$@$Ti_3C_2T_x$-1, and (d) $Co_3V_2O_8$@$Ti_3C_2T_x$-2 electrodes.

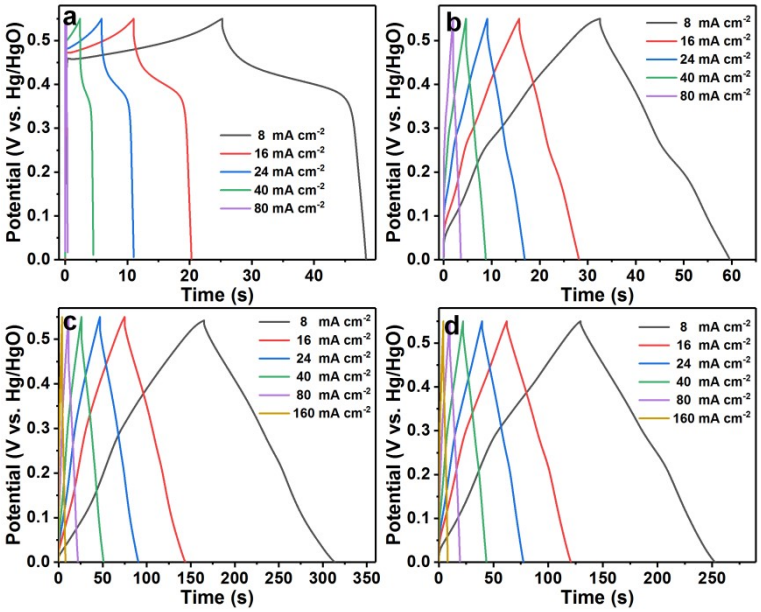

Figure S9. GCD curves for (a) $Ti_3C_2T_x$, (b) pure $Co_3V_2O_8$, (c) $Co_3V_2O_8$@$Ti_3C_2T_x$-1, and (d) $Co_3V_2O_8$@$Ti_3C_2T_x$-2 electrodes.

Table S1. The R_s and R_{ct} values of all electrodes.

Sample	R_s/Ω	R_{ct}/Ω
$Ti_3C_2T_x$	0.80	0.22
$Co_3V_2O_8$	2.19	1.85
$Co_3V_2O_8$@$Ti_3C_2T_x$-1	0.83	0.28
$Co_3V_2O_8$@$Ti_3C_2T_x$-1.5	0.81	0.21
$Co_3V_2O_8$@$Ti_3C_2T_x$-2	2.11	0.42

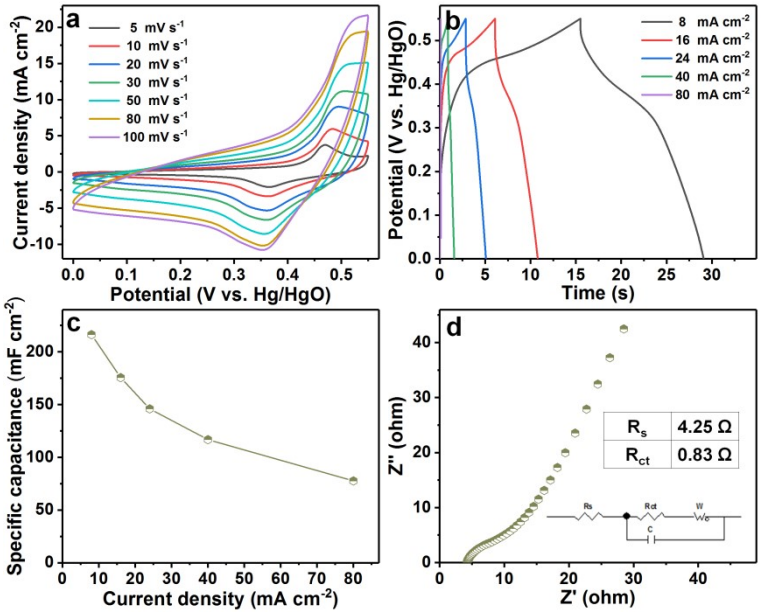

Figure S10. (a) CV curves, (b) GCD curves, (c) specific capacitance at different current densities, and (d) EIS data for the mixture of $Co_3V_2O_8$ and $Ti_3C_2T_x$-1.5 electrode.

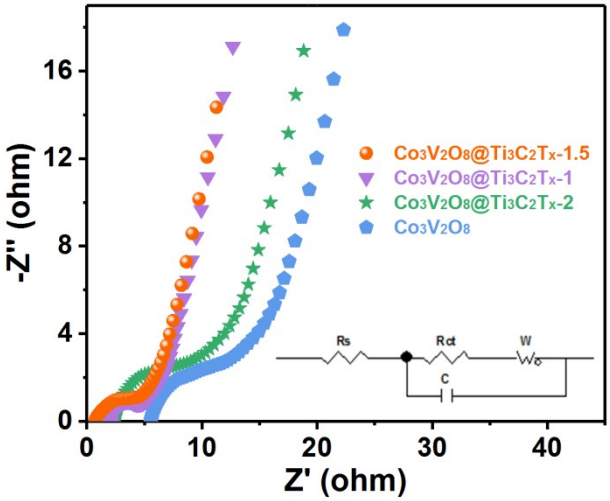

Figure S11. EIS of $Co_3V_2O_8$@$Ti_3C_2T_x$-1.5, $Co_3V_2O_8$@$Ti_3C_2T_x$-1, $Co_3V_2O_8$@$Ti_3C_2T_x$-2, and pure $Co_3V_2O_8$ electrodes after 20000 cycles.

Table S2. The R_s and R_{ct} values of all electrodes after 20,000 cycles.

Sample	R_s/Ω	R_{ct}/Ω
$Co_3V_2O_8$	5.70	2.95
$Co_3V_2O_8$@$Ti_3C_2T_x$-1	2.11	1.56
$Co_3V_2O_8$@$Ti_3C_2T_x$-1.5	0.79	0.69
$Co_3V_2O_8$@$Ti_3C_2T_x$-2	2.46	2.71

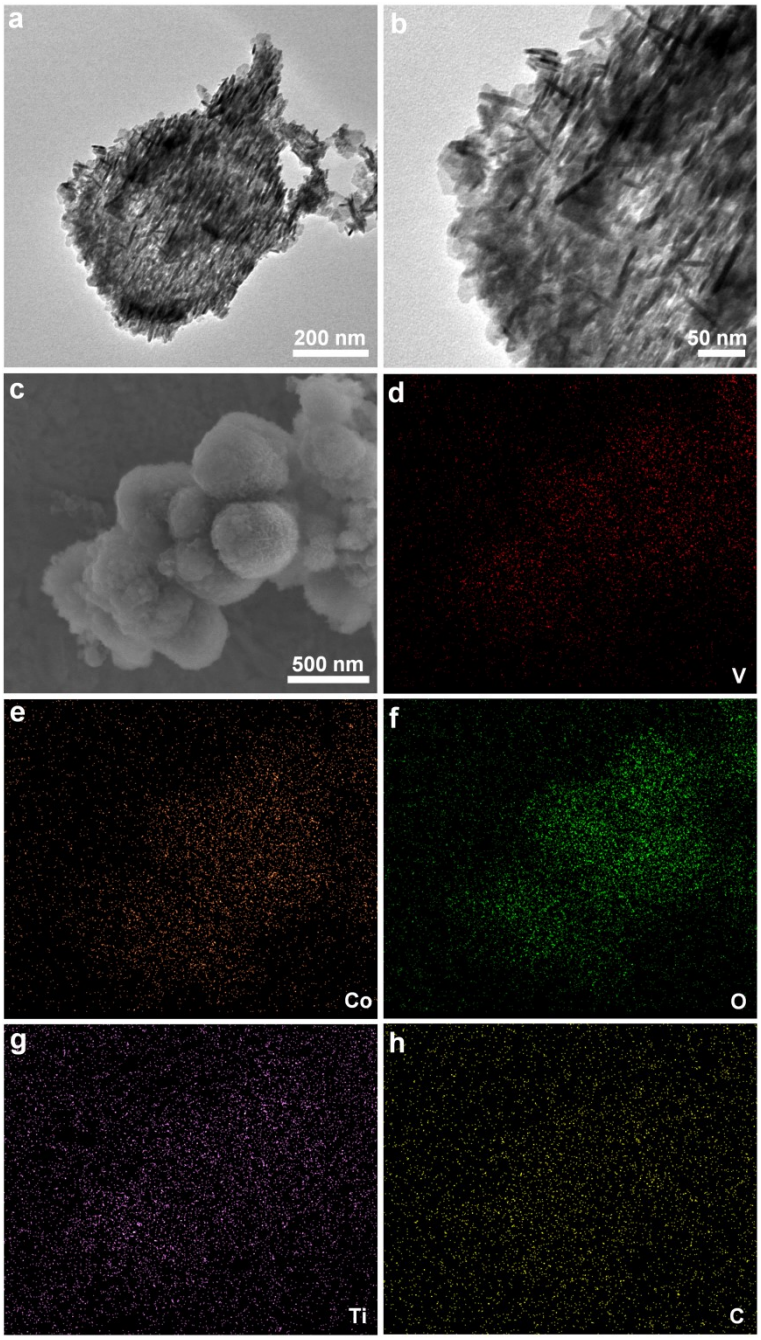

Figure S12. TEM (a, b), SEM (c), and element mapping images (c-h) of $Co_3V_2O_8$@$Ti_3C_2T_x$-1.5 composite after 20,000 cycles.

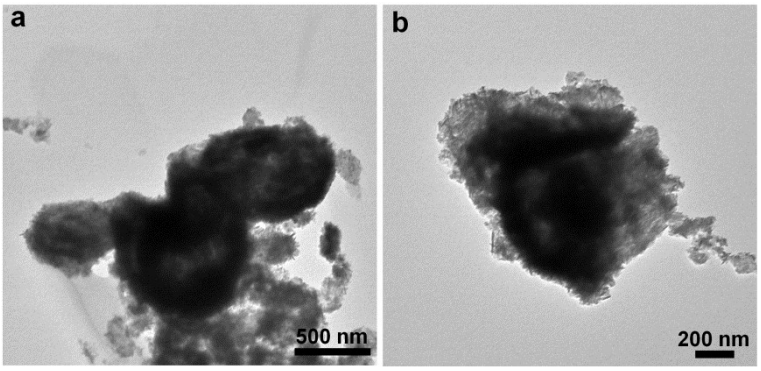

Figure S13. TEM images of pure $Co_3V_2O_8$ sample after 20,000 cycles.

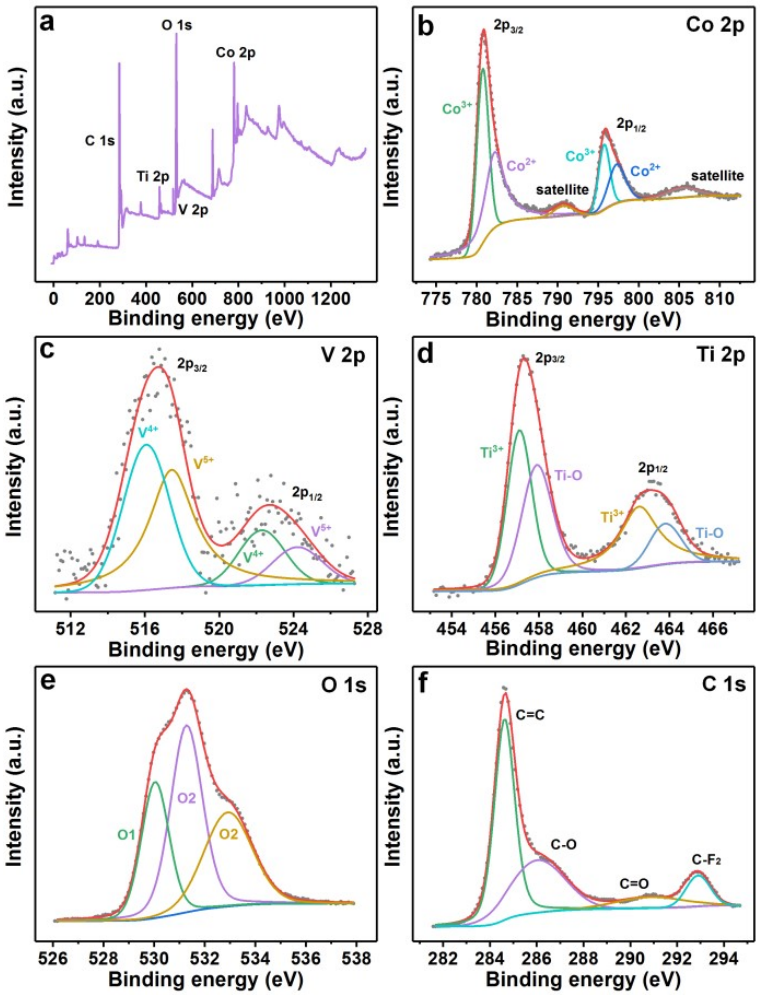

Figure S14. XPS data of $Co_3V_2O_8$@$Ti_3C_2T_x$-1.5 composite after 20,000 cycles.

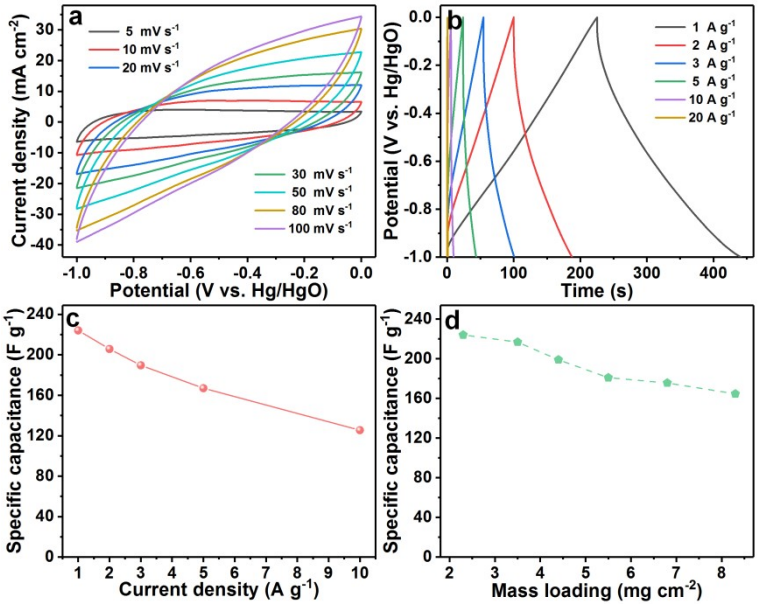

Figure S15. (a) CV curves, (b) GCD curves, (c) specific capacitance at different current densities of the AC anode, (d) specific capacitance of different electrodes with various mass loadings.